

Influence of copper and aluminum substitution on high-temperature oxidation of the FeCoCrNiMn “Cantor” alloy

Mary-Lee Bürckner  | Lukas Mengis | Emma M. H. White  | Mathias C. Galetz 

Materials and Corrosion Division,
DECHEMA Research Institute, Frankfurt
am Main, Germany

Correspondence

Mary-Lee Bürckner, Voltastraße 65
Frankfurt am Main 60486, Germany.
Email: marylee.buerckner@aol.com

Funding information

None

Abstract

In this study, the oxidation behavior of FeCoCrNiMn (HEA + Mn) is compared to three modified HEAs manufactured by substituting Mn with Al, Cu, or Al + Cu. Oxidation tests were conducted between 600°C and 800°C for up to 500 h in synthetic air. Substitution of Mn leads to a significant improvement in the oxidation resistance for the three modified HEAs. For FeCoCrNiCu (HEA + Cu), a local attack of a Cu-rich phase was observed, leading to the formation of CuO blisters on the surface. The FeCoCrNiAl (HEA + Al) alloy was characterized by the formation of a thin Al₂O₃ surface layer for all temperatures. However, for the HEA + Al alloy the formation of AlN was observed after 300 h at 800°C, leading to a partial breakdown of the protective scale. FeCoCrNiCuAl (HEA + Cu + Al) by far showed the best oxidation resistance, characterized by the formation of a highly protective Al₂O₃ scale that effectively inhibited nitrogen penetration into the metal subsurface and local attack of the Cu-rich phase.

KEYWORDS

Al₂O₃ formation, high-entropy alloy, oxidation

1 | INTRODUCTION

High-entropy alloys (HEAs) have experienced a massive increase in popularity among scientists during the last decade. Pioneering work has been done by Cantor et al.^[1] and Yeh et al.^[2] who worked with FeNiCo-based alloys, among others. One of the most famous HEAs is FeCoCrNiMn (known as “Cantor”), which has been extensively examined in regard to its mechanical, corrosive, and oxidation behavior.^[3–5] Although the original definition of HEAs relies on the formation of a single-phased solid solution, stabilized by a high configurational entropy, more recent classifications broadened the definition to include multiphase HEAs based on five or more elements in similar

proportions. Many of these compositions were found not to be single phase.^[3] Despite its high Cr content, the oxidation behavior of the Cantor alloy is determined by Mn as it forms several unprotective oxides which have a fast growth rate due to their high vacancy density.^[4,6] Recent research conducted by Stephan-Scherb et al.^[7] compares FeCoCrNiMn to the oxidation behavior of a CoCrNi model alloy at 800°C. In dry air, only Mn₃O₄ can be detected, while in wet air α-Mn₂O₃ is additionally present. The composition of the oxide is in accordance with Holcomb et al.,^[8] who conducted exposures at 650°C and 750°C in synthetic air. The oxidation resistance of CoCrFeNi was found to be comparable to that of 304H, while the addition of Mn led to higher mass gains and oxide spallation at 750°C. Laplanche et al.^[4] found that a

This is an open access article under the terms of the Creative Commons Attribution-NonCommercial-NoDerivs License, which permits use and distribution in any medium, provided the original work is properly cited, the use is non-commercial and no modifications or adaptations are made.

© 2022 DECHEMA. *Materials and Corrosion* published by Wiley-VCH GmbH.

high temperature (900°C) enhances the formation of Mn_3O_4 , while for lower temperatures, Mn_2O_3 growth dominates.

To date, limited research has been published focusing on the oxidation resistance of HEAs with different compositions. Two descriptive reviews were recently published by Gorr et al.^[9] and Anne et al.,^[6] revealing that besides Cantor, Al-containing HEAs are the second most investigated alloys, as Al is known to improve high-temperature oxidation resistance. Butler et al.^[10] conducted oxidation studies on the $Al_xCoCrFeNi$ system at 1050°C for 100 h. Parabolic kinetics were observed, while a double-layered oxide structure (Al_2O_3 , Cr_2O_3) formed, as well as AlN below the Cr_2O_3 -layer. Al_2O_3 was only prevalent if the Al content was sufficient. In addition, theoretical studies on the $Al_{0.3}CoCrCuFeNi$ alloy, performed by Hong et al.,^[11] underline the importance of the respective Al content to selectively form Al_2O_3 (and not Cr_2O_3) to provide the highest oxidation resistance. They found that oxygen was preferably bound at Cr-rich areas, while Al_2O_3 only developed subsequently.

A previous study on FeCoCrNiMn, FeCoCrNiCu, FeCoCrNiAl, and FeCoCrNiCuAl was conducted by Galetz et al.^[12] on the metal dusting resistance at 620°C of these alloys as Cu and a thermally grown Al_2O_3 scale are known to inhibit carbon ingress into the metal subsurface. It was found that these alloys had significant metal dusting resistance, which makes them promising candidates for high-temperature applications in atmospheres with high carbon activities. However, in addition to their metal dusting resistance, their performance in oxidizing atmospheres at even higher temperatures needs to be investigated to prove their broader industrial viability.

In the framework of this study, isothermal oxidation tests were performed on FeCoCrNiMn, FeCoCrNiCu, FeCoCrNiAl, and FeCoCrNiCuAl at 600–800°C for up to 500 h in dry synthetic air. The primary focus was on the oxide composition, morphology, and subsurface phenomena at 800°C in direct contrast to the well-known FeCoCrNiMn alloy.

2 | EXPERIMENTAL METHODS

FeCoCrNiMn (HEA + Mn), FeCoCrNiCu (HEA + Cu), FeCoCrNiAl (HEA + Al), and FeCoCrNiCuAl (HEA + Cu + Al) samples were produced by the US Department

of Energy's (DOE) Ames National Laboratory (Ames, IA, USA) using an electric arc melting furnace on a water-cooled Cu hearth. The ingots were remelted three times to ensure melt homogenization.

The ingots were wire cut into coupon samples with a size of $3 \times 4 \times 7$ mm, followed by grinding to a P800 grit finish using SiC paper and then cleaned with acetone in an ultrasonic bath. The samples were placed in a quartz glass tube (diameter 4.5 cm) and exposed at 600°C, 700°C, and 800°C for up to 500 h in synthetic air with a flow rate of 4.8 L/h. After exposure, samples were cleaned, sputtered with gold, electrochemically plated with nickel, and embedded in epoxy for further characterization. Some samples showing very porous oxide scales that were prone to spallation were chemically, instead of hot, embedded to ensure the adherence of the oxide scales. Beyond optical microscope investigations, quantitative and qualitative characterization of the oxide layers and the bulk structures was conducted using electron probe microanalysis (EPMA; JXA-8100 manufactured by Jeol) as well as scanning electron microscopy (SEM; SU1000 manufactured by HITACHI equipped with energy-dispersive X-ray spectroscopy [EDS] detector). X-ray diffraction (XRD) measurements with both Cu and Co sources were performed to identify the thermally grown oxide scales of all HEAs, however, the results were unsatisfactory due to the high fluorescence of the bulk materials and were not included.

3 | RESULTS

Alloy chemical compositions were already reported in previous work^[12] and can be obtained from Table 1. HEA + Mn exhibits a single-phase FCC microstructure (Mn segregations are visible only locally) in the as-cast condition at room temperature. In the HEA + Cu alloy substitution of Mn by Cu leads to a two-phase microstructure due to the precipitation of an FCC Cu-rich (45 at%) phase. HEA + Al is characterized by an interdendritic microstructure, which consists of a BCC (19 at% Al/24 at% Cr) and an FCC (13 at% Al/29 at% Cr) phase. For the HEA + Cu + Al alloy, a two-phase BCC + FCC

Material	Abbreviation	Cu	Co	Cr	Fe	Ni	Al	Mn
FeCoCrNiMn	HEA + Mn	-	20.00	19.97	20.00	19.99	-	20.03
FeCoCrNiCu	HEA + Cu	20.01	20.01	20.01	19.98	19.99	-	-
FeCoCrNiAl	HEA + Al	-	19.98	20.02	20.00	19.97	20.04	-
FeCoCrNiCuAl	HEA + Cu + Al	16.65	16.70	16.70	16.68	16.68	16.58	-

TABLE 1 Chemical compositions (from EDS) of the investigated HEAs in at% (adapted from [12])

Abbreviations: EDS, energy-dispersive X-ray spectroscopy; HEA, high-entropy alloy.

microstructure is observed with Cu preferentially segregating to the FCC phase (up to 66 at%).

3.1 | HEA + Mn

The HEA + Mn alloy showed pronounced oxide formation over the entire temperature range which increased with increasing temperature and exposure duration. Figure 1 exemplarily shows a cross section of the HEA + Mn alloy after oxidation at 700°C for 500 h, as well as the corresponding EPMA element maps. The oxide is up to 40 μm thick, porous, and tends to spall off locally while cracks run parallel to the initial surface of the samples. The oxide layer consists of three components: an exterior Mn-rich oxide, followed by a Cr/Co/Fe-rich spinel-type oxide interlayer and a thin Cr₂O₃ layer at the oxide/substrate interface. Several Mn-rich oxide nodules penetrate internally into the substrate leading to an

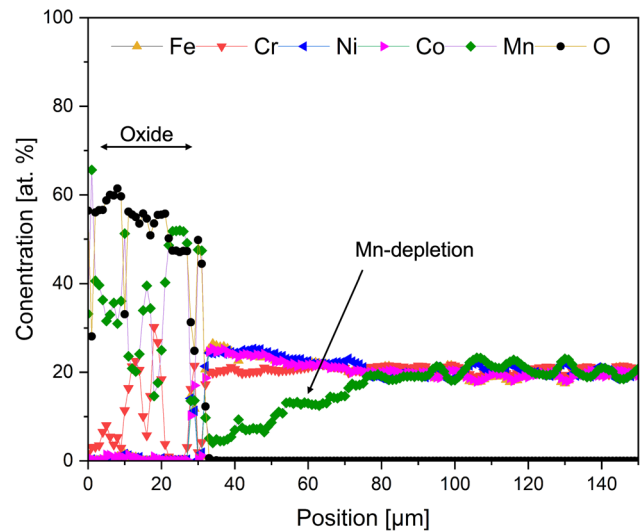


FIGURE 2 EPMA linescan of the HEA + Mn alloy after exposure for 500 h at 700°C in synthetic air. EPMA, electron probe microanalysis; HEA, high-entropy alloy. [Color figure can be viewed at [wileyonlinelibrary.com](https://onlinelibrary.wiley.com/doi/10.1002/maco.202213382)]

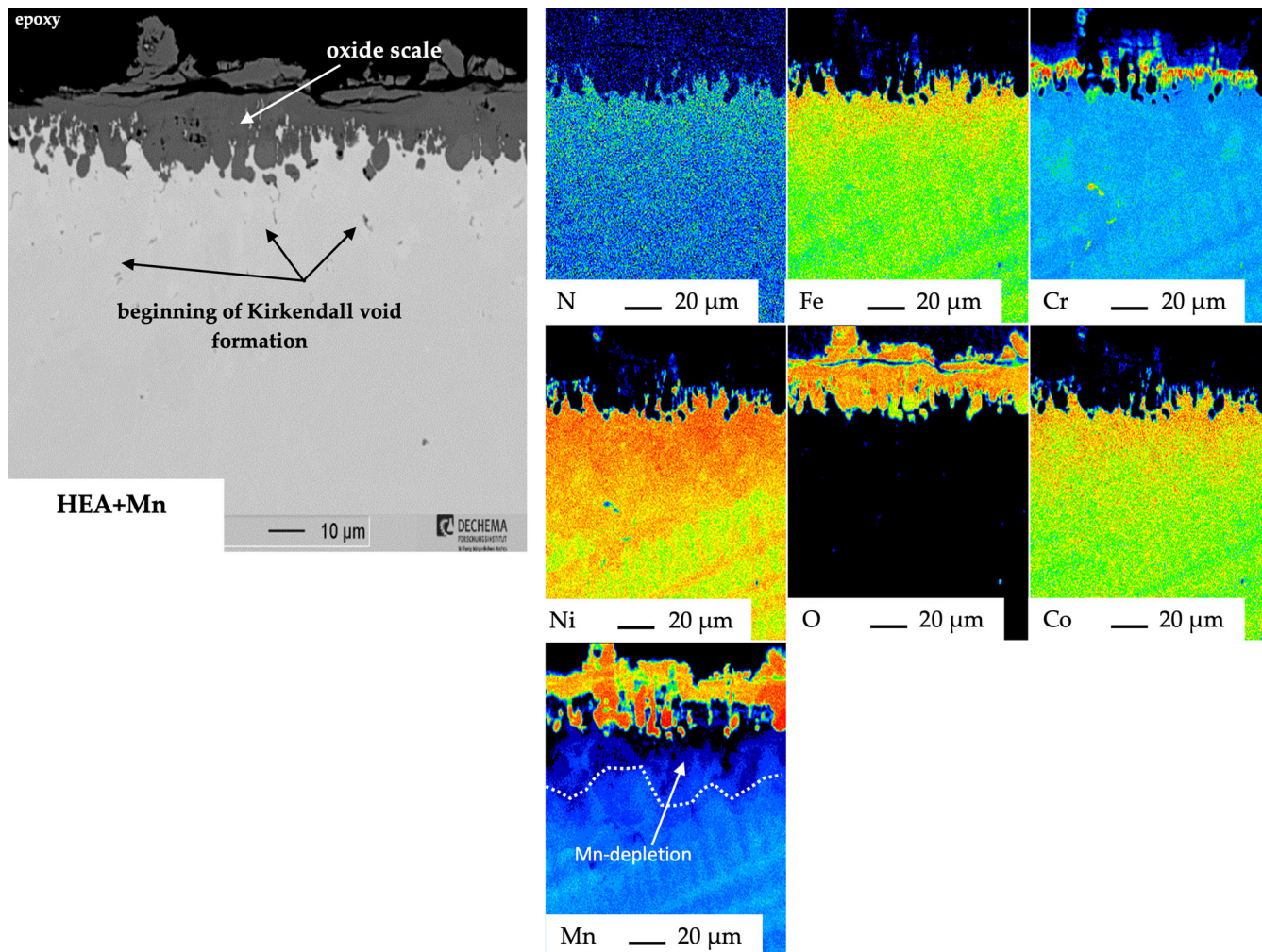


FIGURE 1 Cross-sectional EPMA element maps of the HEA + Mn alloy after exposure for 500 h at 700°C in synthetic air. EPMA, electron probe microanalysis; HEA, high-entropy alloy. [Color figure can be viewed at [wileyonlinelibrary.com](https://onlinelibrary.wiley.com/doi/10.1002/maco.202213382)]

interruption of the Cr_2O_3 layer. The substrate also shows an Mn depletion zone.

Figure 2 shows the corresponding EPMA linescan for the area shown in Figure 1. Mn is heavily depleted for up to 50 μm in the metal subsurface due to fast Mn outward diffusion and Mn oxide formation. In these regions, Kirkendall voids start to form as highlighted in Figure 1. The described oxide morphology and subsurface characteristics accompanied all temperatures/durations and are generally representative of the oxidation behavior of the HEA + Mn alloy.

3.2 | HEA + Cu

At 600°C and 700°C, the HEA + Cu alloy formed a rather thin oxide scale (not shown), however, a selective attack of the Cu-rich phase became evident for all temperatures with longer durations. Using light microscopy, the formation of blisters on top of the surface is apparent, exemplarily shown in the cross section in Figure 3 for the exposure at 800°C. Although most of the surface was covered by a thin scale, blisters exhibiting a metallic appearance were already visible after 100 h and changed color during continued exposure. They preferably grew in areas where the Cu-rich phase had direct contact with the surrounding atmosphere. Their formation was associated with a selective attack of the Cu-rich phase extending into the metal subsurface within approximately the first 20 μm . After 500 h of oxidation, the metallic appearance disappeared, making it difficult to differentiate between the blisters and the “regular” oxide scale.

Figure 4a includes the backscatter electron (BSE) image as well as the corresponding EPMA element maps of the HEA + Cu alloy after oxidation at 800°C for 100 h. Regions in which there was no direct contact between the Cu-rich phase and the atmosphere were covered by a very thin Cr-rich oxide scale, effectively protecting the substrate from further oxidation. Blisters on top of the

surface appeared very bright in BSE mode and showed very low oxygen contents (up to 17.2 at%, EPMA) as well as high Cu contents (up to 84.0 at%, EPMA) leading to the conclusion that they consisted of metallic Cu or Cu_2O . On top of the blisters, as well as in between, darker layers were defined with higher Co-, Cr- and oxygen intensities. Below the blisters, Cu is fully depleted within the former Cu-rich phase and replaced by a Cr/Co/Fe/Ni-rich spinel-type oxide which formed a rather continuous, thin layer between the blisters and the internal Cr_2O_3 . After 500 h (Figure 4b) the bright contrast of the blister was no longer detectable, and the oxygen intensity increased as can be seen in the corresponding EPMA map. Additionally, EPMA spot measurements within the blisters (up to 52.0 at% Cu) showed rather high oxygen contents (up to 47.3 at%). Regions of the surface without direct contact with the Cu-rich phase were still covered by a rather thin Cr-rich oxide scale, that was partially overgrown by a Fe-/Co-/Cu-rich scale. The internal oxidation proceeded up to about 50 μm deep in the metal subsurface and was characterized by severe Cu-depletion. Cr_2O_3 formed at the interface between the former Cu-rich phase, hindering oxygen penetration further into the base material.

3.3 | HEA + Al

For the HEA + Al alloy, a homogenous Al_2O_3 -layer formed for all temperatures and times. An increase in temperature led to a slight increase in oxide thickness, however, the oxide layer remained significantly thinner than for the previously described HEA + Mn or HEA + Cu alloys for all exposures. The protective nature of the Al oxide was clearly visible after oxidation for 100 h at 800°C (Figure 5). Below the Al_2O_3 scale, an Al-depleted region was even more pronounced after oxidation for 300 h and contained internal nitridation. There was not a significant difference in the appearance of the external and internal scale formation between 300 and 500 h.

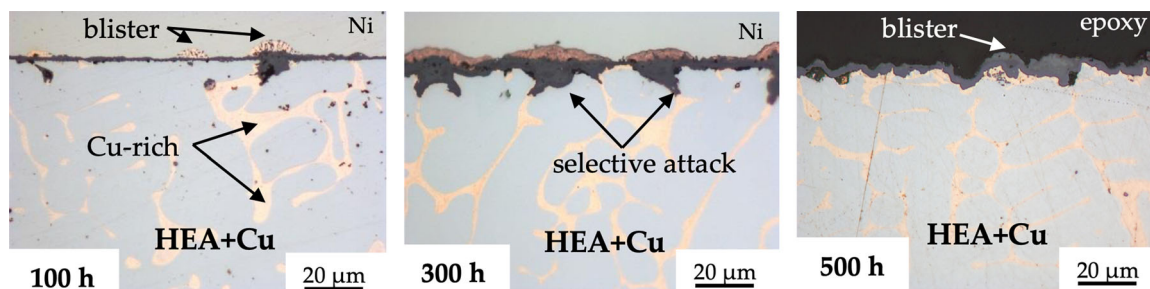


FIGURE 3 Cross-sectional light microscope images of the HEA + Cu alloy after exposure at 800°C for 100, 300, and 500 h in synthetic air. HEA, high-entropy alloy. [Color figure can be viewed at [wileyonlinelibrary.com](https://onlinelibrary.wiley.com/doi/10.1002/maco.202213382)]

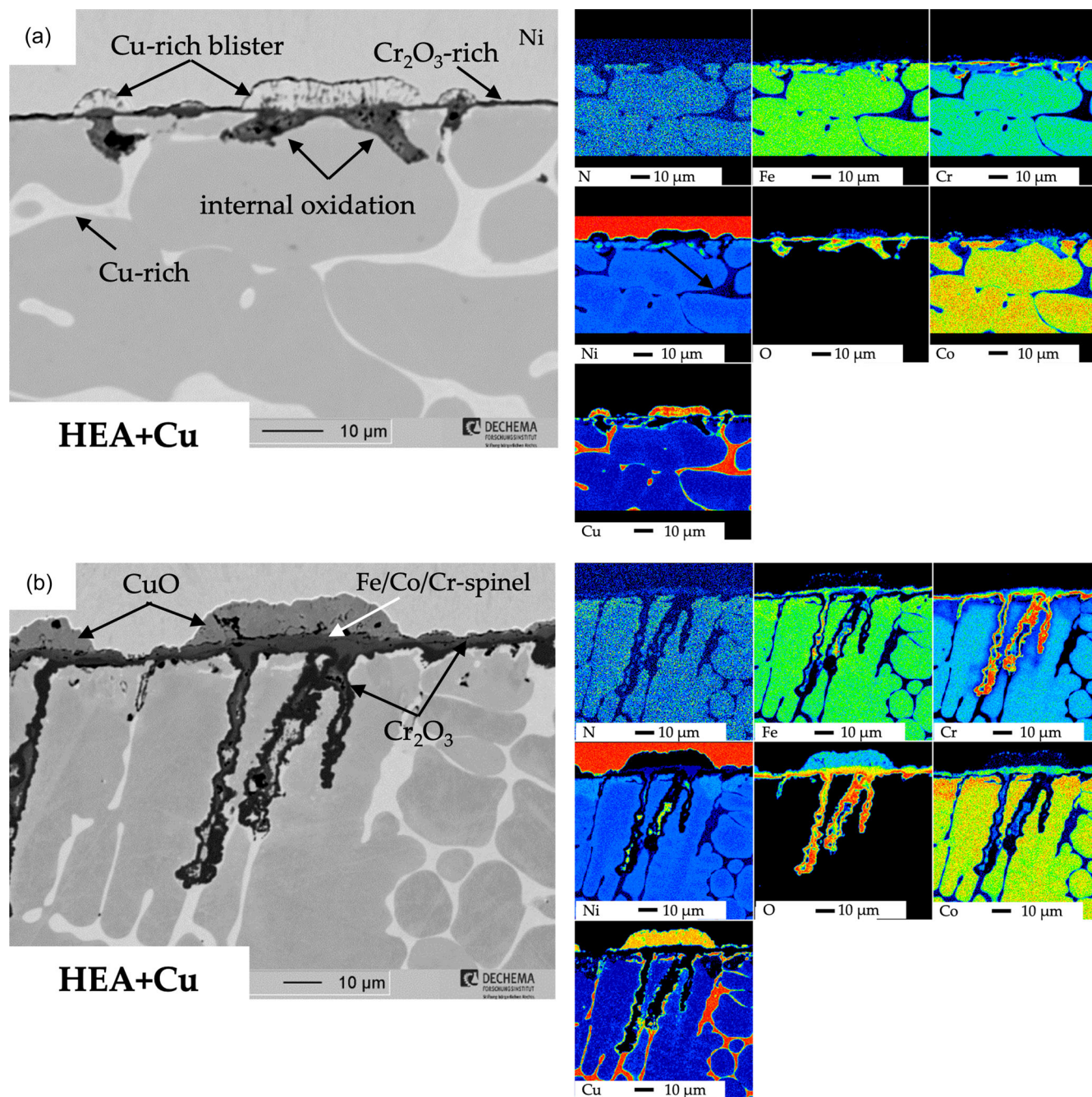


FIGURE 4 Cross-sectional EPMA element maps of the HEA + Cu alloy after exposure for (a) 100 h and (b) 300 h at 800°C in synthetic air. EPMA, electron probe microanalysis; HEA, high-entropy alloy. [Color figure can be viewed at [wileyonlinelibrary.com](https://onlinelibrary.wiley.com/doi/10.1002/maco.202213382)]

The respective EPMA element maps in Figure 6 revealed internal AlN nitride formation in the Al-depleted subsurface zone although the external Al_2O_3 -scale seemed to be rather homogeneous and protective. Higher Cr- and Fe-intensities in the external oxide scale were only seen locally in regions where the AlN formation was even more pronounced. There was no evidence for AlN-formation at 600°C and 700°C for the entire duration of exposure.

3.4 | HEA + Cu + Al

Similar to the HEA + Al alloy, a protective Al_2O_3 layer with a subsurface Al-depletion zone formed on the HEA + Cu + Al alloy for all temperatures and exposure durations. The oxide layer was very homogeneous, crack-free, and thin, even after exposure at 800°C for 500 h (Figure 7). The local attack of the Cu-rich phase was greatly inhibited, occurring only infrequently and not

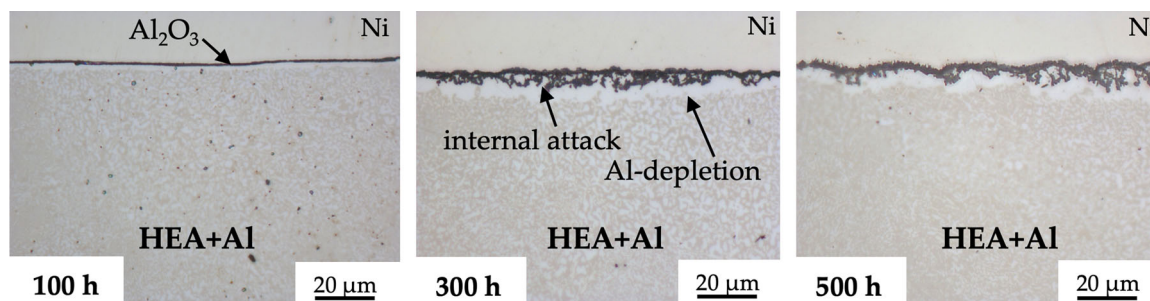


FIGURE 5 Cross-sectional light microscope images of the HEA + Al alloy after exposure at 800°C for 100, 300, and 500 h in synthetic air. HEA, high-entropy alloy. [Color figure can be viewed at [wileyonlinelibrary.com](https://onlinelibrary.wiley.com/doi/10.1002/maco.202213382)]

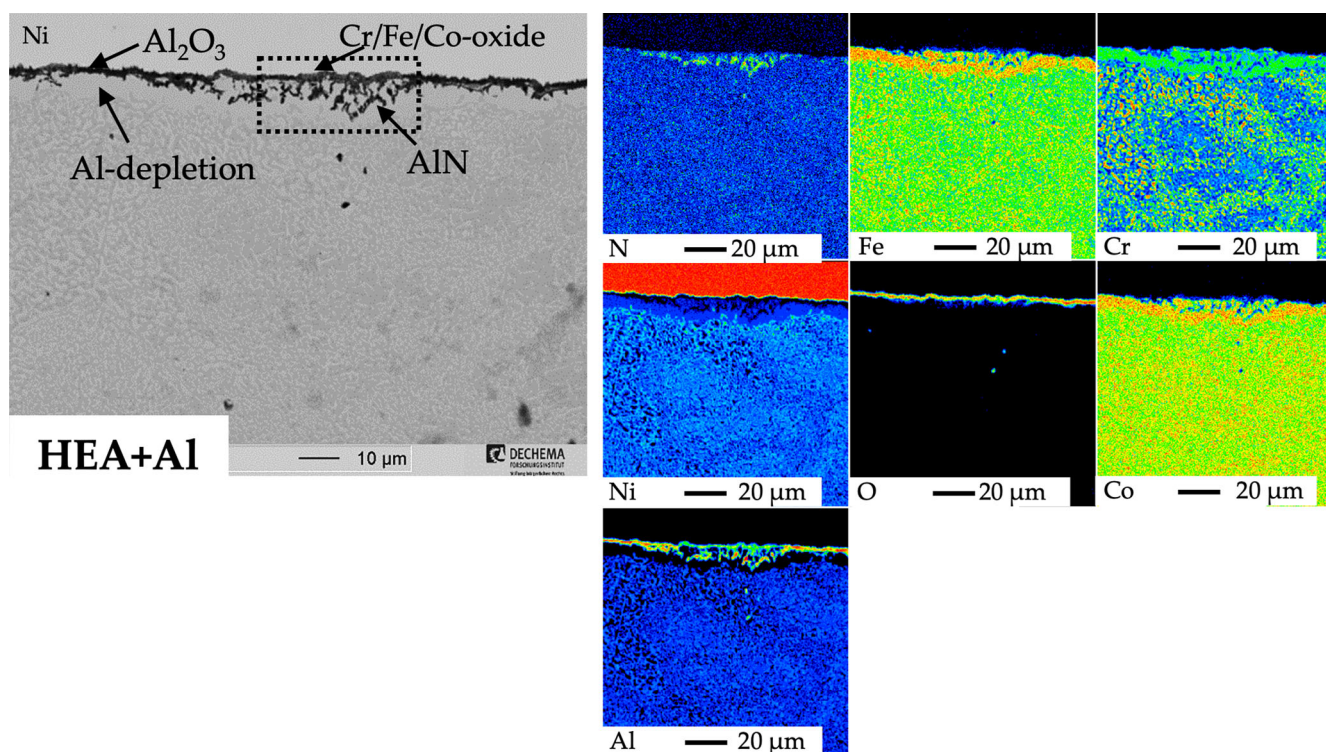


FIGURE 6 Cross-sectional EPMA element distribution maps of the HEA + Al alloy after exposure at 800°C for 500 h in synthetic air. EPMA, electron probe microanalysis; HEA, high-entropy alloy. [Color figure can be viewed at [wileyonlinelibrary.com](https://onlinelibrary.wiley.com/doi/10.1002/maco.202213382)]

extending deep into the material, as was the case for the HEA + Cu alloy.

The Al depletion was also prevalent for the HEA + Cu + Al samples and increased with increasing time and/or temperature. In contrast to the HEA + Al alloy, the formation of AlN was never observed as can be seen in Figure 7 for exposure at 800°C for 500 h. In the cross section in Figure 8, microstructural changes occurred in the bulk which became even more pronounced with increasing temperature. These changes were clearly visible in the Cr, Ni, and Al maps in Figure 9 and similarly occurred for the HEA + Al alloy (not shown). In the given temperature range, the formation of the

γ' -phase is expected.^[13] However, for both alloys, it could not be observed based on stoichiometric analysis due to the small diameter of the γ' -phase. For nickel-based alloys such as alloy 263, γ' precipitates have diameters below 100 nm when heat treatment is below 800°C, which cannot be resolved by the methods used in this study.^[13] Between 300°C and 850°C, the presence of σ -phase has been found for Al_{0.5}CoCrCuFeNi.^[14] For the alloy composition used in this study, the formation of the σ -phase could also be confirmed previously by XRD.^[12] However, both microstructural changes are finely phase dispersed and thus do not appear to have a significant influence on the oxidation behavior in this study.

4 | DISCUSSION

4.1 | HEA + Mn

The oxidation behavior of the HEA + Mn (“Cantor”) alloy has been studied extensively in literature as described previously.^[4,7,8,15] The observations from this

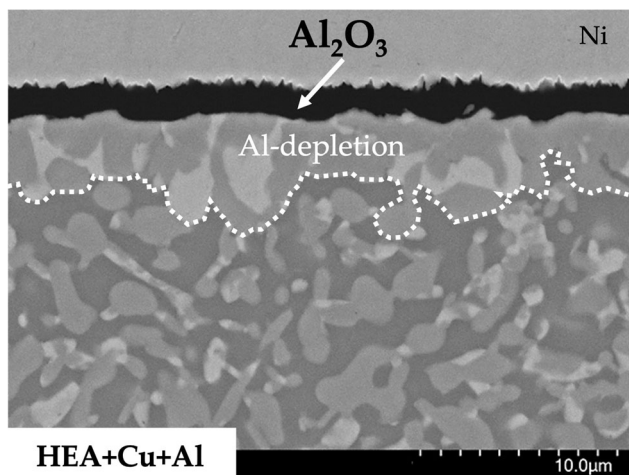


FIGURE 7 BSE image of the HEA + Cu + Al alloy after exposure for 300 h at 800°C in synthetic air. BSE, backscatter electron; HEA, high-entropy alloy.

study align well with the results described in the literature.^[4,7,8,15] The poor oxidation resistance is primarily caused by fast Mn oxide growth rates which are already prevalent at 600°C. The Mn outward diffusion is much higher than for Cr, Ni, and Co.^[16] Besides a Mn oxide, an Fe/Co/Cr spinel with a rather high oxidation rate was formed, resulting in a complex intermixed outer oxide scale as can be seen in Figure 1. The fast diffusion of Mn leads to severe Mn depletion (Figure 2) and the formation of Kirkendall voids in the metal subsurface. Kirkendall voids form in the case of differences in the diffusion rates of the alloying elements and can cause the preliminary delamination of thermally grown oxide scales.^[17] A proposed schematic illustration of the oxidation process in dry synthetic air is shown in Figure 9. The exact composition of the spinel is difficult to determine since it varies locally and the atomic radii of the included elements (Fe, Cr, Mn) are similar. The basic oxide composition as well as the respective oxidation state of the Mn oxide might also vary under the influence of water vapor or temperature as has been recently proposed by Stephan-Scherb et al.^[7]

It is important to note the process of Cr₂O₃ formation in the HEA + Mn alloy. As Mn, as well as Fe and Co, are successively consumed due to their higher outward diffusion and thus external oxide scale formation,

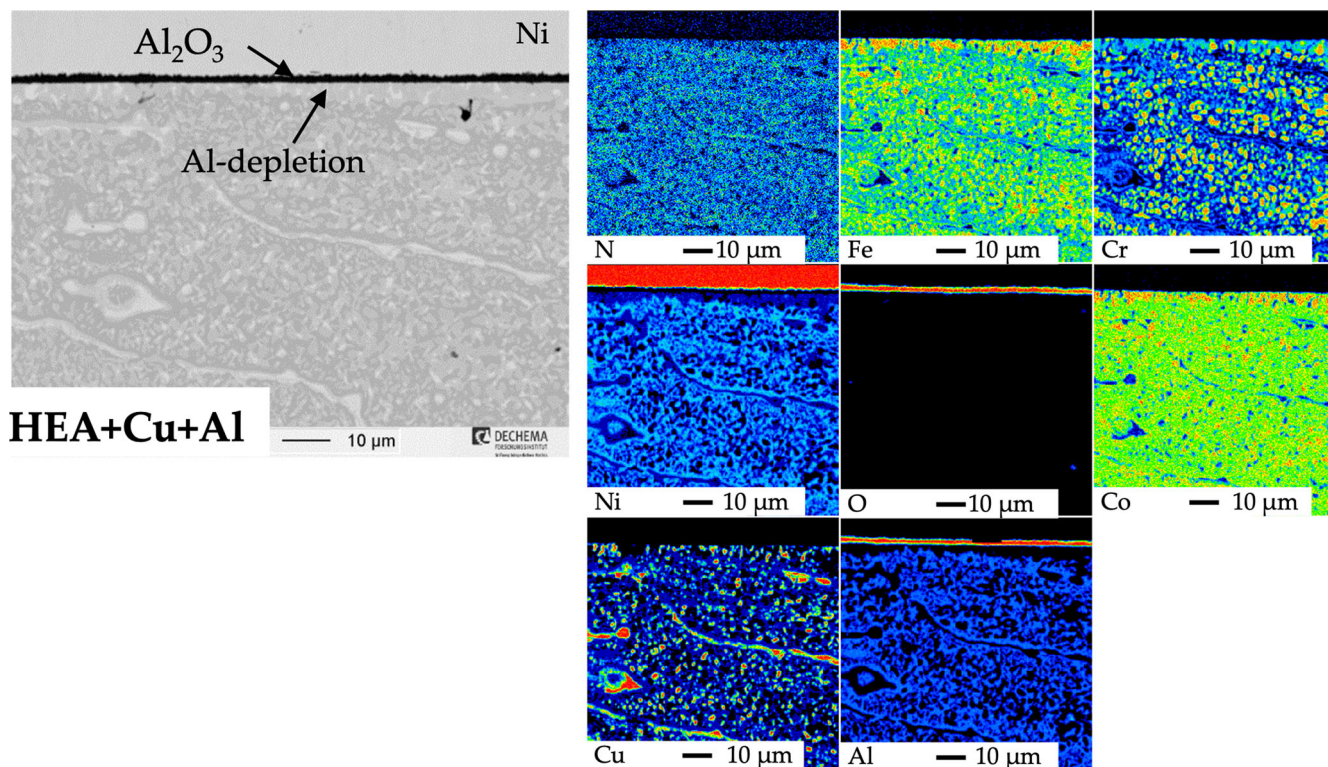


FIGURE 8 Cross-sectional EPMA element distribution maps of the HEA + Cu + Al alloy after exposure for 500 h at 800°C in synthetic air. EPMA, electron probe microanalysis; HEA, high-entropy alloy. [Color figure can be viewed at [wileyonlinelibrary.com](https://onlinelibrary.wiley.com)]

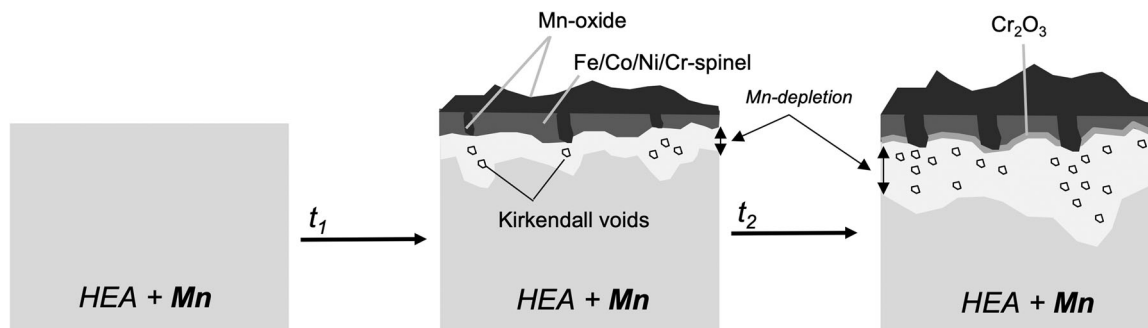


FIGURE 9 Proposed high-temperature oxidation mechanism of the HEA + Mn alloy as a function of time. HEA, high-entropy alloy.

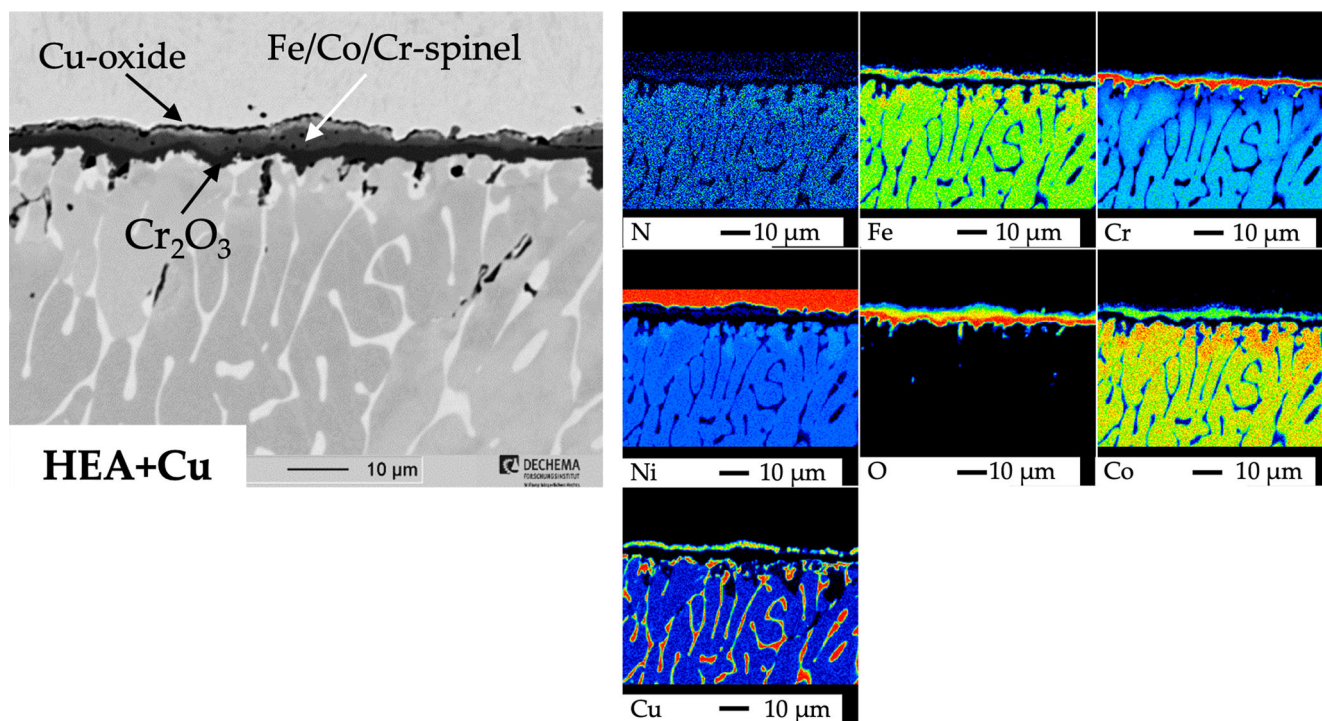


FIGURE 10 BSE image of a Cu-lean region of the HEA + Cu alloy after oxidation at 800°C for 500 h in synthetic air with corresponding EPMA element maps. BSE, backscatter electron; EPMA, electron probe microanalysis; HEA, high-entropy alloy. [Color figure can be viewed at [wileyonlinelibrary.com](https://onlinelibrary.wiley.com/doi/10.1002/maco.202213382)]

Cr enriches in the inner part of the oxide scale over time, similar to 9 wt% Cr steel after breakaway.^[18] However, despite the high Cr content in the alloy, the Cr-rich oxide (composition suggesting Cr₂O₃) layer is interrupted by inner Mn oxide nodules and therefore can only protect the substrate to a certain extent.

4.2 | HEA + Cu

Substitution of Mn by Cu leads to the formation of a Cu-rich phase (FCC) and, therefore, a two-phase microstructure.^[15] When analyzing the oxidation behavior of the HEA + Cu alloy, one must carefully distinguish

between the oxidation resistance of both phases, subsumed as Cu-rich and Cu-lean in the following. For the Cu-lean phase, the oxidation behavior is primarily characterized by the formation of rather thin scales which consist of an outermost Cu oxide, followed by an Fe/Co/Cr-spinel interlayer and a continuous Cr₂O₃ layer at the interface to the substrate (a triplex oxide). To further clarify this description, Figure 10 shows a BSE image with corresponding EPMA element maps of the HEA + Cu alloy after oxidation at 800°C for 500 h. The formation of continuous Cr₂O₃ at the interface effectively protects the alloy from further oxidation.

The oxidation behavior of the Cu-rich phase is quite complex and further metallographic investigations

(e.g., transmission electron microscopy) would be necessary to fully clarify the occurring phenomena. The proposed oxidation mechanism is shown schematically in Figure 11 as a function of time (constant T) and is representative of the entire temperature range from 600°C to 800°C. Two explanations are conceivable from a thermodynamic and kinetic point of view and are presented in the following.

For the first potential explanation, oxidation is theorized to take place in multiple distinctive oxidation–reduction steps. After oxidation for 100 h, a local attack of the Cu-rich phase leads to the formation of blisters with a metallic appearance in the light microscope on top of the surface (Figure 3). Due to the low oxygen and high Cu content, in combination with the overall very low oxygen solubility of Cu,^[19] it can be assumed that these blisters are metallic or at least only partially oxidized. As there must be a driving force for Cu to diffuse out of the matrix, intermediate oxidation of Cu presumably leads to the formation of Cu_2O on the surface. The simultaneous formation of a very thin spinel layer on top of the blister, below, and also in between, in combination with its slightly higher thermodynamic stability, could lead to a partial reduction of Cu_2O to Cu_{met} . With increasing time, oxidation leads to the formation of CuO which is the most stable Cu oxide.^[20] The successive consumption of Cu leads to an even more pronounced spinel formation below the CuO and, finally, inhibition of further oxidation by protective Cr_2O_3 . According to the ternary Cu–Cr–O phase diagram, for example in [21], Cr and Cu also form a spinel and inverse spinel, however, they were not detected using EPMA, suggesting that their formation is either kinetically unfavorable or thermodynamically impossible in the complex system with the other elements forming Cr-spinels, which were found, such as Mn and Co.

For the second potential explanation, subsurface Cu is selectively pushed out of the matrix due to internal spinel formation, leading to an increase in volume. Due to the limited space, metallic blisters form on the surface,

which eventually oxidize to CuO . Thermodynamically, Cr_2O_3 , as well as the spinel, are more stable than the Cu oxides, and thus Cr_2O_3 finally forms below the spinel where the oxygen partial pressure is lower. This aspect highlights the importance of Cr as a protective oxide-forming element in this HEA family.

4.3 | HEA + Al

The two-phase (BCC + FCC) HEA + Al alloy shows significantly better oxidation resistance compared to the previously described alloys. Figure 12 summarizes the proposed oxidation behavior of HEA + Al schematically. Even after exposure at 800°C for 100 h in synthetic air the extremely thin Al_2O_3 layer remains stable and protects the base material from severe oxidation (Figure 5a). With increasing time at 800°C, the formation of needle-like AlN was observed in the Al-depleted region below the Al_2O_3 (Figure 5b,c). Nitrogen from the atmosphere must have diffused through microcracks or pores of the outer Al_2O_3 layer to be able to penetrate the metal subsurface and react with Al. The formation of AlN is unsurprising as Al is a strong nitride former.^[22] Thermal stresses in the oxide or ongoing transformation processes from metastable to stable Al_2O_3 could have caused such defects. For HEA + Al, nitridation was observed also by Butler et al.^[10] as well as Dabrowa et al.^[23] and seems to be a general phenomenon for Al-containing HEAs. As Figure 6 already implies, Cr, Fe, and Co start to oxidize and grow over the Al_2O_3 layer in the regions where the AlN formation is most pronounced. As Al is trapped by AlN formation, Cr, Fe, and Co are enriched in the subsurface. The protectiveness of the oxide is weakened since the mixed oxide shows higher oxidation rates compared to Al_2O_3 at the tested temperatures. The spinel is also susceptible to evaporation due to its Cr content in the form of CrO_3 (at around 1000°C^[24]) and volatilization in water vapor-containing atmospheres at even lower temperatures.^[25] The investigation of the oxidation

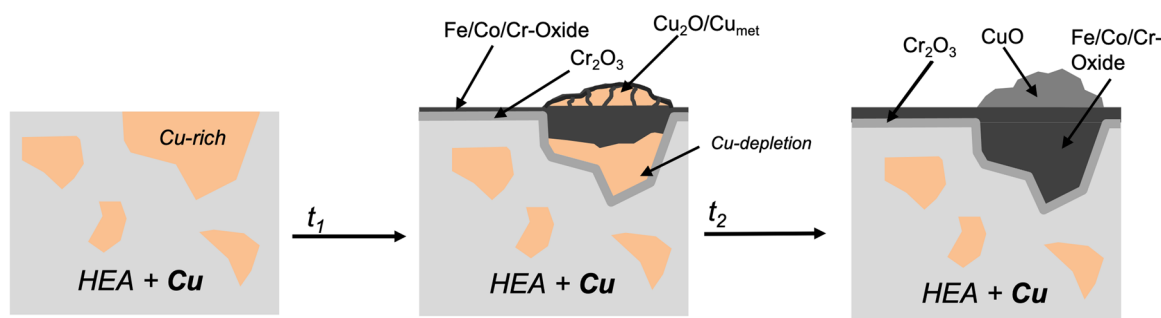


FIGURE 11 Proposed high-temperature oxidation mechanism of the HEA + Cu alloy as a function of time. HEA, high-entropy alloy. [Color figure can be viewed at [wileyonlinelibrary.com](https://onlinelibrary.wiley.com/doi/10.1002/maco.202213382)]

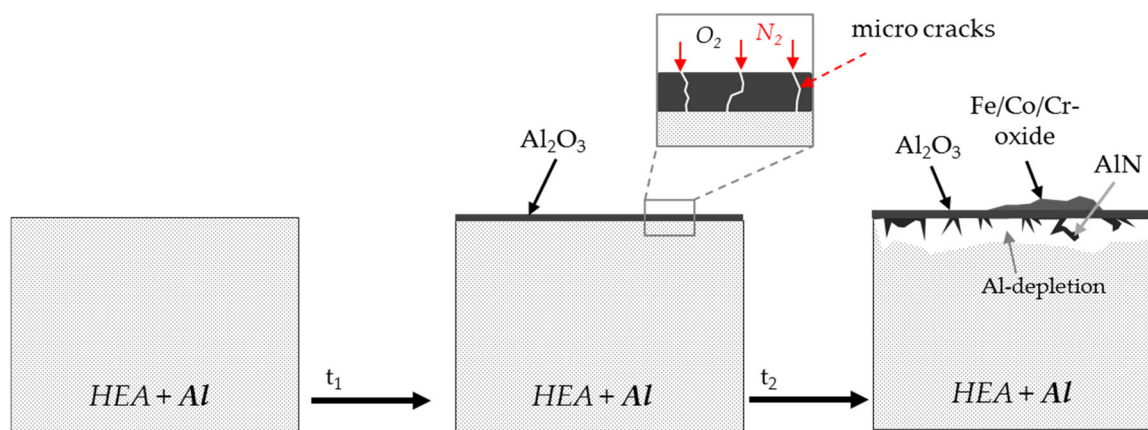


FIGURE 12 Proposed high-temperature oxidation mechanism of the HEA + Al alloy as a function of time. HEA, high-entropy alloy. [Color figure can be viewed at [wileyonlinelibrary.com](https://onlinelibrary.wiley.com/doi/10.1002/maco.202213382)]

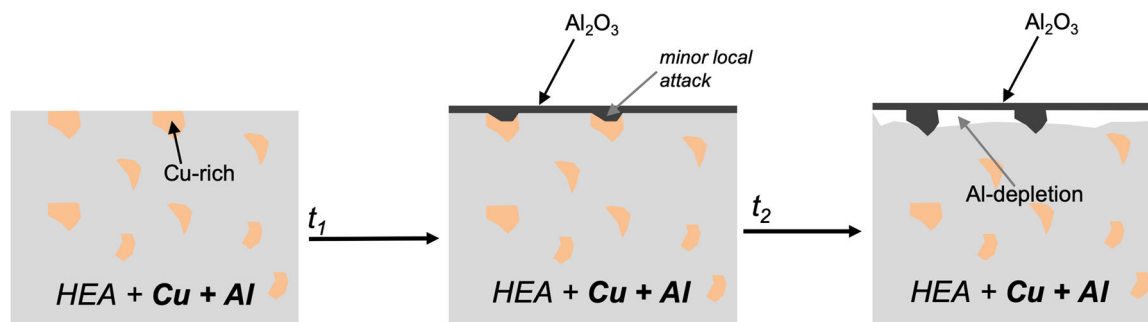


FIGURE 13 Proposed high-temperature oxidation mechanism of the HEA + Cu + Al alloy as a function of time. Observed microstructural changes in the bulk are neglected. HEA, high-entropy alloy. [Color figure can be viewed at [wileyonlinelibrary.com](https://onlinelibrary.wiley.com/doi/10.1002/maco.202213382)]

behavior for even longer exposure durations (>1000 h) or under the presence of water vapor should be conducted in future work to investigate the long-term stability of the alloy.

4.4 | HEA + Cu + Al

The HEA + Cu + Al alloy by far shows the best oxidation behavior among the four HEA alloys due to the selective oxidation of Al over the entire temperature range (Figure 7). The proposed oxidation mechanism is schematically shown in Figure 13. In comparison to HEA + Cu, the local attack of the Cu-rich phase is negligible since the Al_2O_3 scale forms before Cu can react. This protection is enhanced by the overall smaller diameter of the Cu-rich phase in the HEA + Cu + Al alloy compared to HEA + Cu (due to the lower Cu content^[12]) which indicates the initial microstructure is a contributing factor, not only for mechanical purposes but also when it comes to the oxidation behavior at high temperatures. Additionally, the formation of a spinel

seems to be effectively suppressed. In comparison to the HEA + Al alloy, there is no evidence for AlN formation below the oxide scale (and, therefore, Cr_2O_3 growth), even after oxidation at 800°C for 500 h (Figure 8). One potential explanation is small amounts of Cu in the Al_2O_3 scale might minimize thermal stress generation or accelerate the transformation from metastable to stable $\alpha\text{-Al}_2\text{O}_3$ (and therefore reducing the number of microcracks) inducing a so-called “third-element-effect.”^[26] Additionally, Cu in a solid solution could affect the diffusion of Al throughout the multiphase microstructure. Detailed investigation of this phenomenon needs further metallographic analysis using high-resolution techniques.

As is also the case for the HEA + Al alloy, microstructural changes are expected for the HEA + Cu + Al alloy after high-temperature exposure. By increasing the temperature from 600°C to 800°C the phase transformation becomes even more pronounced. The formation of σ -phase, which is typical for austenitic alloys, was previously observed by Galetz et al.^[12] already after exposure at 620°C or by Laplanche^[27] for the CrMnFeCoNi HEA.

The precipitation of the σ -phase could generally lead to significant embrittlement of the material as is the case for austenitic Fe-base alloys.^[28] In direct contrast, HEA + Mn, for example, retains a single-phase microstructure during exposure. While structural changes potentially strongly influence the mechanical behavior of the alloy, the oxidation behavior seems to be less affected within this study. This could be due to the sufficient Al content of both Al-containing HEAs. While Cr is absent in the Cu-rich phase, Al is prevalent in both phases (>5 at% in the Cu-rich phase, up to 15 at% in the Cu-lean phase). It must be mentioned that Cr gets trapped to a large extent within the σ -phase (Figure 8) and therefore is no longer available for oxide scale formation in case of detrimental failure of the outer Al_2O_3 scale. This trapping of a protective oxide former is very similar to the one observed within this study when AlN developed and thus spinels with higher growth rates formed instead.

5 | CONCLUSIONS

The oxidation behavior of FeCrMnNiCo (HEA + Mn) as a reference alloy, as well as FeCrNiCoCu (HEA + Cu), FeCrNiCoAl (HEA + Al), and FeCrNiCoCuAl (HEA + Cu + Al), was investigated in the temperature range of 600–800°C for up to 500 h in synthetic air. The major findings can be summarized as follows:

- HEA + Mn showed poor oxidation resistance due to the fast growth of Mn oxide (along with Mn depletion and Kirkendall void formation in the subsurface) and a complex spinel at 600°C. The subscale Cr-rich layer was frequently interrupted by internally growing Mn oxide nodules and therefore cannot effectively protect the alloy from further oxidation.
- HEA + Cu had a two-phase microstructure and clearly showed improved oxidation resistance compared to HEA + Mn, characterized by the formation of a triplex oxide scale (CuO/spinel/ Cr_2O_3). Selective attack of the Cu-rich phase and the formation of blisters on top of the surface, which fully oxidize to CuO, occurred after longer oxidation times (300–500 h).
- In the HEA + Al alloy substitution of Mn by Al led to very good oxidation resistance at 600°C and 700°C due to the formation of a protective Al_2O_3 layer. At 800°C, AlN formation was observed after 300 h below the outer Al_2O_3 scale. Microcracks within the oxide scale presumably facilitate local nitrogen ingress into the Al-depleted metal subsurface and engender local breakdown of the otherwise very protective scale.
- HEA + Cu + Al clearly showed the best oxidation resistance among the four examined alloys due to the

formation of a protective Al_2O_3 layer with long-term stability. No nitridation nor Cu blister formation were observed which makes the HEA + Cu + Al alloy a promising candidate for high-temperature applications in both oxidizing and carbon-containing atmospheres.

ACKNOWLEDGMENTS

EPMA measurements were conducted by Dr. Gerald Schmidt at DECHEMA DFI. Materials for this study were provided by the “Science-based Acceleration of the Full Value Stream for Metal Additive Manufacturing: Expedited AM Powder Development (X-P4AM)” project funded by the U.S.DOE-EERE-AMO through Ames Lab contract DE-AC02-07CH11358.

DATA AVAILABILITY STATEMENT

The data that support the findings of this study are available from the corresponding author upon reasonable request.

ORCID

Mary-Lee Bürckner  <http://orcid.org/0000-0002-5820-9806>

Emma M. H. White  <http://orcid.org/0000-0002-0246-6256>

Mathias C. Galetz  <http://orcid.org/0000-0001-6847-2053>

REFERENCES

- [1] B. Cantor, *Entropy* **2014**, *16*, 4749.
- [2] J. W. Yeh, *JOM* **2013**, *65*, 1759.
- [3] D. B. Miracle, O. N. Senkov, *Acta Mater.* **2017**, *122*, 448.
- [4] G. Laplanche, U. F. Volkert, G. Eggeler, E. P. George, *Oxid. Met.* **2016**, *85*, 629.
- [5] E. P. George, D. Raabe, R. O. Ritchie, *Nat. Rev. Mater.* **2019**, *4*, 515.
- [6] B. R. Anne, S. Shaik, M. Tanaka, A. Basu, *SN Appl. Sci.* **2021**, *3*, 366.
- [7] C. Stephan-Scherb, W. Schulz, M. Schneider, S. Karafiludis, G. Laplanche, *Oxid. Met.* **2021**, *95*, 105.
- [8] G. R. Holcomb, J. Tylczak, C. Carney, *JOM* **2015**, *67*, 2326.
- [9] B. Gorr, S. Schellert, F. Müller, H. J. Christ, A. Kauffmann, M. Heilmaier, *Adv. Eng. Mater.* **2021**, *23*, 2001047.
- [10] T. M. Butler, M. L. Weaver, *J. Alloys Compd.* **2016**, *674*, 229.
- [11] Y. Hong, M. Beyramali Kivy, M. Asle Zaeem, *Scr. Mater.* **2019**, *168*, 139.
- [12] M. C. Galetz, C. Schlereth, E. M. H. White, *Mater. Corros.* **2021**, *72*, 1232.
- [13] D. Gianfrancesco, *Materials for Ultra-Supercritical and Advanced Ultra-Supercritical Power Plants*, Woodhead Publishing, Duxford, UK **2017**, pp. 571.
- [14] C. Ng, S. Guo, J. Luan, S. Shi, C. T. Liu, *Intermetallics* **2012**, *31*, 165.
- [15] N. K. Adomako, J. H. Kim, Y. T. Hyun, *J. Therm. Anal. Calorim.* **2018**, *133*, 13.
- [16] K. Y. Tsai, M. H. Tsai, J. W. Yeh, *Acta Mater.* **2013**, *61*, 4887.

- [17] D. J. Young, *High Temperature Oxidation and Corrosion of Metals*, 1st ed., Elsevier, Amsterdam, the Netherlands **2008**.
- [18] M. Schütze, M. Schorr, D. P. Renusch, A. Donchev, J. P. T. Vossen, *Mater. Res.* **2004**, *7*, 111.
- [19] L. Schramm, G. Behr, W. Löser, K. Wetzig, *J. Phase Equilibria Diffus.* **2005**, *26*, 605.
- [20] Z. Grzesik, M. Migdalska, *High Temp. Mater. Process.* **2011**, *30*, 277.
- [21] J. Hamuyuni, P. Taskinen, *Thermochim. Acta.* **2016**, *638*, 96.
- [22] E. Lewin, *J. Appl. Phys.* **2020**, *127*, 160901.
- [23] J. Dąbrowa, G. Cieślak, M. Stygar, M. Zajusz, M. Jawańska, A. Gil, J. Jedliński, K. Mroczka, K. Matsuda, T. Kulik, M. Danielewski, *Oxid. Met.* **2021**, *96*, 307.
- [24] H. Asteman, J. E. Svensson, L. G. Johansson, *Oxid. Met.* **2002**, *57*, 193.
- [25] D. J. Young, B. A. Pint, *Oxid. Met.* **2006**, *66*, 137.
- [26] F. H. Stott, G. C. Wood, J. Stringer, *Oxid. Met.* **1995**, *44*, 113.
- [27] G. Laplanche, *Acta Mater.* **2020**, *199*, 193.
- [28] C.-C. Hsieh, W. Wu, *Int. Sch. Res. Notices.* **2012**, *2012*, 16.

How to cite this article: M.-L. Bürckner, L. Mengis, E. M. H. White, M. C. Galetz, *Mater. Corros.* **2023**;74:79–90.
<https://doi.org/10.1002/maco.202213382>